Deformation, Yield and Fracture of Elastomer-Modified Polypropylene

S. M. Zebarjad,[1] R. Bagheri,[1] S. M. Seyed Reihani,[1] A. Lazzeri[2]

[1]*Department of Materials Science and Engineering, Sharif University of Technology, Azadi Avenue, 14584, Tehran, Iran*
[2]*Center for Materials Engineering, University of Pisa, Via Diotisalvi 2, 56126 Pisa, Italy*

Received 27 February 2002; accepted 14 February 2003

ABSTRACT: In recent decades, great attention has been devoted to the toughening of isotactic poly(propylene) (PP) with elastomers such as ethylene–propylene rubber (EPR). The most important reasons for this interest are the moderate cost and favorable properties of PP. This article is focused on the role of EPR in the deformation and fracture mechanism of PP/EPR blends with different volume fractions of elastomer phase. Differential scanning calorimetry (DSC), tensile tests, and microscopy techniques were used in this study. The fracture mechanism of isotactic PP toughened by EPR (PP/EPR) has also been studied by three point bending (3-PB) and four point bending (4-PB) tests. Rubber particle cavitation appears to be the main mechanism of microvoid formation, although some matrix/particle debonding was observed. The investigation of the toughening mechanism shows that a wide damage zone spreads in front of the pre-crack. Optical microscopy (OM) illustrates that, in pure PP, crazing is the only fracture mechanism, and no evidence of shear yielding is found, while in PP blends craze-like features associated with shear yielding are observed, which have been identified as high shear localized dilatational bands. This type of deformation pattern supports a model previously proposed by Lazzeri[1] to explain the interparticle distance effect on the basis of the stabilization effect on dilatational band propagation exerted by stretched rubber particles. © 2003 Wiley Periodicals, Inc. J Appl Polym Sci 90: 3767–3779, 2003

Key words: poly(propylene) (PP); elastomers; toughness; mechanical properties; particle size distribution

INTRODUCTION

The increasing market demand for moderately priced, recyclable engineering plastics has made poly(propylene) (PP) an attractive candidate for numerous applications. PP is produced in a wide variety of types, characterized by melt flow indices (MFI) ranging from 0.3 to more than 1000 g/10min. In addition to the ease of processing by virtually all methods, including injection molding, blow molding, extrusion and thermoforming, PP can be easily recycled.[2-3] Nevertheless, because of the poor impact strength of pure PP, its use in automotive and other engineering applications is still limited compared to its potential.

Rubber toughening is a well-established method of improving fracture toughness. Polypropylene is most often toughened by feeding ethylene into the reactor near the end of the polymerization, so that about 10 vol % of ethylene–propylene copolymer is formed *in situ*. This 'copolymer' grade of PP is in fact a rubber-toughened version of PP. Blending of rubbers such as ethylene–propylene rubber (EPR), ethylene-propylene-diene monomer rubber (EPDM), Styrene Butadiene Styrene (SBS), Styrene Ethylene Butadiene Styrene (SEBS), Polybutadiene (PB) or Polyisoprene (PiP) with PP homopolymer or copolymer grade can also be carried out in a batch mixer after polymerization to further improve the impact strength. PP/EPR blends have applications in the automotive industry, including the manufacture of bumpers and dashboards.[2-3]

A recent paper reviewed several aspects of the toughening of semicrystalline thermoplastics, including isotactic PP,[4] and a specific review has been devoted to the rubber toughening of PP.[5] From these reviews, it appears that the major theories explaining the toughening mechanisms of these blends are multiple crazing, shear-yielding, and the formation of microvoids due to rubber cavitation or debonding from the matrix. Moreover, the factors affecting toughening appear to be quite complicated, because the addition of a rubbery phase affects the nucleation of crystals during solidification from the melt.[6] Therefore, these theories appear to be valid only in some cases when they are applied under relevant conditions, and no general consensus on the subject been reached.

An aspect that remains under debate is the controversial critical interparticle distance effect proposed almost twenty years ago by Wu.[7] In fact, this concept is strongly correlated to several critical processing parameters, like the optimum particle size distribution and the morphological structure of the elastomer

Correspondence to: A. Lazzeri (a.lazzeri@ing.unipi.it).

Journal of Applied Polymer Science, Vol. 90, 3767–3779 (2003)

phase. These parameters play a crucial role in the design of new polymer blends and composites, particularly in the selection of a surface treatment that allows the formation of a suitable interface or interphase and determines the proper level of adhesion.

The study reported in this article is part of a larger series devoted to the explanation of the mechanical behavior of complex mineral-filled, short-fiber reinforced and rubber-toughened PP systems used in automotive applications.[8–10]

In particular, the aim of this study is to further understand the role of rubber particles in deformation and fracture mechanism in PP/rubber. Furthermore, the question of the formation of high-shear localized dilatational bands will be studied in relation to a previous model that takes into account the load bearing capability of rubber particles.

EXPERIMENTAL

Materials

A series of PP blends was used in this study. Pellets of 'copolymer' grade PP containing 20 wt % EPR (corresponding to 20.8% by volume), with the trade name Hifax CA 35M, were obtained from the Montell company (Ferrara, Italy). According to the manufacturer, the EPR phase contains 70 wt % ethylene. The average size of the EPR particles is about 3.5 μm, with bigger particles measuring approximately 4–6 μm.

To produce pellets containing 16 wt % (16.62 vol %) and 8 wt % (8.34 vol %) rubber, the original blend was diluted with isotactic PP with a MFI of 8 (g/10 min) from Imam Khomeini Petrochemical Complex (trade name 080) and extruded in a Windsor SX-30 single-screw extruder (Windsor Machine & Stamping, Windsor, Ontario, Canada) at a screw speed of 60 rpm over a temperature range of 180–220°C.

Standard tensile specimens were made via injection molding. The temperature in the four successive zones of the Mono-mat 80 injection molding equipment (Eckert & Ziegler GmbH, Weißenburg, Germany) was increased progressively along its length from 200 to 230°C.

Tensile tests

Tensile tests were carried out according to ASTM D638 using an 1115 Instron tensile frame at a crosshead speed of 5 mm/min (corresponding to a strain rate of 0.03 s^{-1}). A minimum of three samples per material was tested at room temperature. In order to investigate the dominant deformation mechanism during tensile tests, the side surfaces of some samples were polished prior to the test to achieve a surface roughness of about 5 μm. After the desired degree of deformation was achieved, polished surfaces were studied by means of optical and scanning electron microscopes. Also in order to clarify the mechanism of deformation, after testing, some samples were cold fractured in liquid nitrogen along the tensile direction. The new fracture surfaces were subsequently investigated by scanning electron microscopy (SEM).

Three-point bending test

An endemic problem when dealing with rubber toughened polymers is that upon increasing rubber content, the materials become progressively tougher, and the conditions for linear elastic fracture mechanics (LEFM) are no longer met. So the original 'copolymer' grade PP and the materials with lower rubber content were tested according to the 1990 testing protocol approved by European Structural Integrity Society (ESIS) to obtain the plane strain fracture toughness, K_{IC}.[11] For the two blends with higher rubber content, *J*-testing was performed according to the ESIS protocol,[12] making use of a multispecimen technique to measure the *J*-resistance curves and the fracture toughness, J_{IC} (considered here to be equivalent to $J_{0.2}$) at room temperature. The corresponding K_{IC} value has been calculated by using the following formula:

$$K_{IC} = \sqrt{E \cdot J_{IC}}$$

where E is the Young's modulus.

All fracture toughness tests were carried using single edge notched 3-point bending (SEN-3PB) geometry, using a 1115 Instron tensile frame at a crosshead speed of 1 mm/min. Pre-cracks were produced by means of a razor blade, which had been previously chilled at low temperature.

Specimens for K_{IC} testing were prepared according to the testing protocol: length (L) = 60 mm, width (W) = 12.7 mm, thickness (B) = 6 mm, span (S) = 50.8 and the initial notch depth, (α_0) = 6.0 mm. For J_{IC} testing, the same sample dimensions were used.

To elucidate the behavior of samples during the test, the side surfaces of some samples (without pre-crack) were polished prior to testing. After some deformation occurred, those surfaces were studied via optical and SEM.

Four-point bending test

In order to observe the crack tip damage zone of PP and PP blends, the double edge-notched four point bending (DEN-4PB) geometry was employed. For this test, a 1115 Instron tensile frame was used at a crosshead speed of 1 mm/min. The sample thickness was 6 mm. Other relevant geometrical parameters are reported in Figure 1. Details of this technique are as follows. First, two edge cracks of equal length were

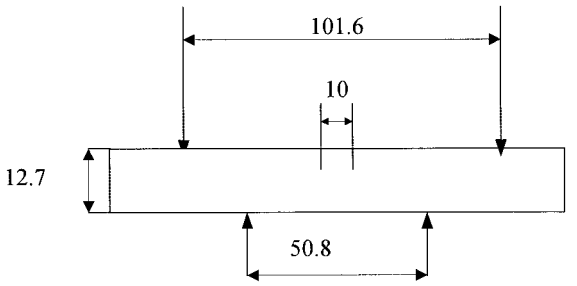

Figure 1 Schematic of four-point bending test specimen.

introduced into the bending samples. In order to protect the specimens from mechanical work after testing, the side surfaces of the samples were polished prior to testing to achieve a surface roughness of about 1 μm. Then each specimen was loaded into a four-point bending fixture until damage zones formed near the crack tips. Finally, one of the two cracks reached the instability condition and propagated until the final fracture of the sample. After completion of fracture, the other crack unloads, thus leaving a well-developed damage zone that clearly represents the condition of the material just before failure. The surface of the damage zone can be observed using optical and SEM.

To investigate the damage zone under plane strain condition, it would be necessary to observe the interior of the samples by using transmission optical microscopy (TOM). This can be achieved by thinning the sample to about 30–50 μm via petrographic polishing.[13] The procedure used in this work, in which the microscope examination is limited to the external surfaces of the samples and thus plane stress regions are visible, has two main advantages, however: (a) protection of the specimen from mechanical damage during the thinning and polishing stages, and (b) relative ease of operation. Since this optical microscopy study is complemented by SEM analysis of the fracture surface, the overall examination of the results can provide an accurate picture of the fracture mechanism operating in the materials under investigation.

Microscope evaluation

PM3 and BX60 Olympus optical microscopes were employed to examine the damage zone in tensile and DN-4PB specimens, respectively, under reflective light conditions. Also, an Olympus SZ40 optical microscope was used to measure the stress whitening width. A Jeol JSM-5600LV scanning electron microscope was used to study the side surfaces of 3PB and 4PB bars and the fracture surfaces of selected samples. The specimens were coated, using an Edwards S150B sputter coater, with a thin layer of gold prior to microscopy to avoid charge build up.

Calorimetric analysis

Thermal properties were measured using a Perkin-Elmer DSC-2C differential scanning calorimeter. The instrument was calibrated by measuring the melting temperature of indium. All measurements were performed under nitrogen flow. The mass of the samples used varied between 5 and 8 mg. During the first heating run, which was performed at the rate of 10°C/min, the temperature range examined was from room temperature to somewhere higher than the melting point of the samples. After reaching this temperature, the specimens were cooled at the same rate of 10°C/min. The second heating run was performed similarly at the rate of 10°C/min. Temperatures and heats of melting (crystallization) were determined from the melting peaks and from the corresponding areas of the thermograms, respectively. The degree of crystallinity was calculated from the heat of fusion, assuming a value of 209 J/g as the enthalpy of fusion of a perfect (100%) isotactic PP crystal.[14]

RESULTS AND DISCUSSION

Thermal behavior

The melting behavior of pure PP and its blends is summarized in Table I. The results show that pure PP and PP blends exhibit an endothermic peak, indicating the absorption of heat during the melting process. The amount of heat developed during the melting phase of PP in the blend is almost independent of the rubber content. The degree of crystallinity of the PP phase in all blends is estimated to be about 50%. The increase of crystallization temperature with increase of rubber

TABLE I
DSC Data

Rubber content (wt %)	Heating I			Heating II			Cooling	
	Tm (°C)	ΔHm (J/g PP)	ΔHm (J/g blend)	Tm (°C)	ΔHm (J/g PP)	ΔHm (J/g blend)	Tc (°C)	ΔHc (J/g)
0%	166.69	105.1	105.1	166.7	103.1	103.1	111.39	−109.1
8%	164.9	107.2	98.7	166.1	107.9	99.27	113.23	−94.8
16%	164.9	107.4	90.3	165.3	108.1	90.8	115.25	−91.8
20%	164.3	106.5	85.2	164.0	107.7	86.2	117.15	−90.2

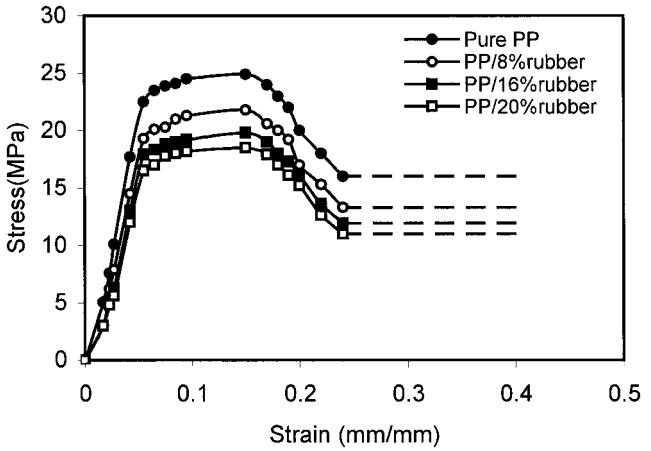

Figure 2 Dependence of tensile behavior on rubber content.

content can be attributed to the nucleation effect of elastomer particles on PP crystallization, because they decrease the average size of spherulites,[15] encouraging PP fracture resistance.[16]

Tensile behavior

The stress–strain curves of pure PP and PP blends are shown in Figure 2. As seen, increasing rubber content reduces the yield stress and the Young's modulus but does not change the tendency of the material to neck and draw. In fact, the necking phenomenon was observed in all samples, including pure PP and PP blends. Figures 3 and 4 demonstrate the variations of tensile modulus and yield stress as a function of rubber content, respectively. In these figures, the measured values of Young's modulus and yield stress of the blends studied are compared to the predictions of the Nielsen[17] and the Lazzeri and Bucknall equations,[18] respectively.

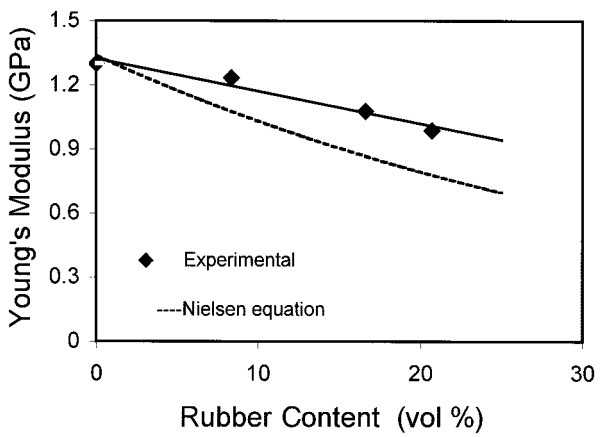

Figure 3 Variation of Young's modulus with rubber content.

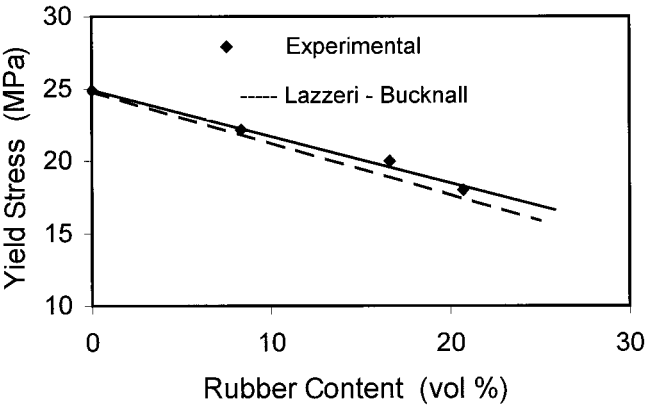

Figure 4 Variation of yield stress with rubber content.

By modifying the original Kerner equation, Nielsen proposed for the blend shear modulus, G, the following expression[17]:

$$G = G_m(1 - B_e\psi\varphi_e)/(1 + A_eB_e\varphi_e) \quad (1)$$

where G_m is the matrix shear modulus, and φ_e is the volume fraction of the dispersed phase, while

$$A_e = (8 - 10\ \nu_m)/(7 - 5\ \nu_m) \quad (2)$$

$$B_e = (G_m - G_e)/(G_m + A_eG_e) \quad (3)$$

and ψ takes into account the maximum packing fraction of the dispersed phase:

$$\psi = 1 + \{(1 - \varphi_e{}^{\max})/(\varphi_e{}^{(\max)2})\}\varphi_e \quad (4)$$

In the above expressions, G_e is the shear modulus of the filler, ν_m is the Poisson ratio of the matrix and $\varphi_e{}^{\max}$ is the maximum packing fraction of the dispersed phase. The Young's modulus can be deduced from the shear modulus via eq. (5):

$$E = 2G(1 + \nu) \quad (5)$$

The values of the parameters used for the calculations are listed in ref.19.

The reasons for choosing the relatively simple Nielsen equation are basically the fact that although many attempts have been made since Nielsen's original work[17] to model the elastic behavior of rubber-modified blends and, more generally, of composite materials containing spherical inclusions, these studies prove that the problem is extremely difficult to solve. In real blends, the particles are distributed both in their size and in their spatial distribution, even if they are all spherical. Satisfactory solutions are therefore almost impossible to obtain. The best that can be done, ad example the Reuss equation[20] and the Es-

helby inclusion method of Chow,[21] define just upper and lower bounds on the modulus. This is equally true of modern work on modulus, based on finite-element analysis (FEA). These approaches work for regular arrays of identical spherical particles dispersed in a continuous matrix, but not for real blends, with all of their irregularities. Good results from analytical expressions or FEA require the exact concentration of dispersed particles to be known and likewise the properties of both phases to be known precisely. The precise determination of these parameters is beyond the scope of this article, so the relatively unsophisticated Nielsen's equation was considered reasonable for a first approach analysis of the experimental data. Moreover, the modified Kerner's equation is frequently used by workers in the field of mineral filler reinforced polymers.[20]

Comparison of theoretical and experimental values of Young's moduli show similar trends upon increasing the rubber content (Fig. 3). However, the theoretical expression underestimates the modulus data. As discussed above, the Nielsen equation cannot take into account important factors, such as particle size distribution and level of adhesion between matrix and rubber phase.

Regarding the yield stress of PP/EPR blends, according to Lazzeri and Bucknall[18]

$$\sigma_Y = \sigma_0(1 - 1.375\varphi_e) \quad (6)$$

where σ_Y and σ_0 are the yield stresses of the blend and the matrix, respectively, and φ_e is the volume fraction of the dispersed phase.

As seen in Figure 4, there is a good fit between the experimental data and the suggested equation, on the basis of their modified Gurson's yield function by Lazzeri-Bucknall,[18] which was shown to fit very well some experimental data by Gloagen and coworkers[22] and verified later by FEA.[23] This is quite interesting, since this equation was derived from compression test results, where particle cavitation does not occur. Lazzeri and Bucknall[18] showed that, under the condition of low triaxiality, there is only a small difference between the effect of non-cavitated particles and voids and cavitated particles on the tensile yield stress, especially at low volume fractions, those below 20%.

The reason both modulus and yield stress decrease with increasing rubber content can be attributed to the fact that, since rubber particles have very low shear modulus compared to PP, there is little or no stress transfer from matrix to elastomer particles. Therefore, particles have almost the same effects as micro-voids on these mechanical properties.

Optical microscopy of deformed tensile bars

Figure 5(a,b) shows optical micrographs of the polished surfaces of tensile bars of pure PP and a blend containing 20 wt % rubber, respectively, after some stretching. As can be seen in these figures, a large number of craze-like features are observed in the gauge length. Experiments show that the number of these features increases during plastic deformation until saturation occurs within the gauge length, wherein a neck forms prior to the rupture of the specimen. The density of the damage decreases when moving away from the necking shoulder in specimens. It can also be observed that increasing rubber content or level of deformation promotes the tendency to damage intersection. The results of this study illustrate that craze-like damage in PP blends can be initiated by EPR particles, while in pure PP it is formed in the bulk.

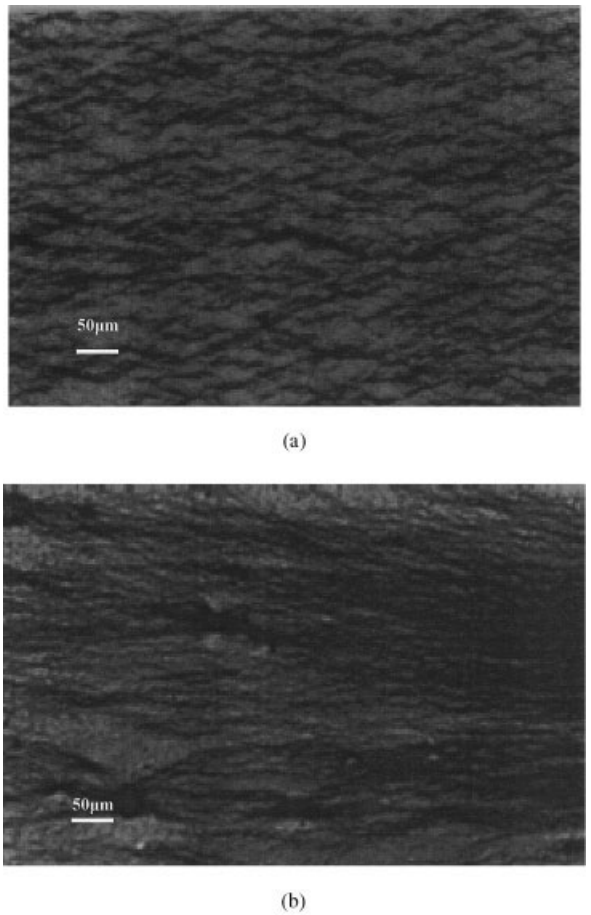

Figure 5 Optical microscopy of polished surfaces of tensile specimens after some deformation, showing the damage in (a) pure PP and (b) PP/EPR blend. The loading direction is vertical.

Electron microscopy of deformed and fractured tensile bars

To further elucidate the deformation mechanisms, and in particular the nature and structure of the craze-like bands observed in optical microscopy, electron microscopy was employed. Figure 6(a,b) shows SEM micrographs of the polished side surfaces of tensile

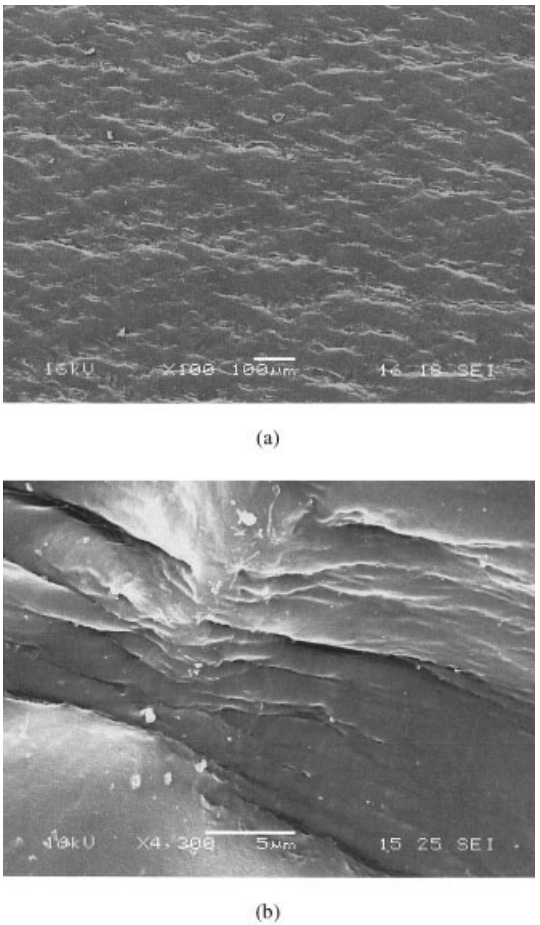

Figure 6 SEM micrographs of polished surfaces of tensile specimens of pure PP, showing (a) a general view of the damage zone and (b) detail of a deformation band.

specimens of pure PP. As seen in these figures, there are some craze-like features with different lengths [Fig. 6(a)]. These craze-like structures, unlike normal crazes, deviate from the normal direction of the applied load, even by more than 25° [Fig. 6(a)] and show some similarities to shear bands [Fig. 6(b)].

Figure 7(a–d) shows scanning electron micrographs of the polished side surfaces of tensile specimens made with the PP/EPR (20 wt %) blend. Figure 7(a) shows a view of the specimen surface after some stretching. As can be seen, damage forms at some points and then propagates in different directions. Figure 7(b–d) are blow-ups of Figure 7(a). In these figures, some elongated voids are observed, which are probably formed due to cavitation of rubber particles. Figure 8(a,b) shows the fracture surfaces of the tensile bars of the same PP blend.. While some elongated voids formed due to rubber particle debonding are clearly visible in Figure 8(a), particle cavitation appears to be the dominant mode, with cavities preferentially arranged along lines, as seen in Figure 8(b). Analyzing all of these micrographs and particularly comparing Figures 8(a) and 7(d), one may conclude that the deformation mechanism in tensile deformation for PP blends is massive shear dilatational banding due to repeated cavitation.

Fracture characterization: 3-PB tests

Figure 9 shows that fracture toughness steadily increases with rubber content. A few words must be devoted to the fracture toughness values presented in this work. Considering the yield stress data measured for these materials, neither K_{IC} nor J_{IC} tests on our EPR/PP blends meet the size limitations given by the two test protocols[11-12] for plane strain fracture parameter determination. For example, the thickness required for K_{IC} samples of pure PP should be in excess of 14 mm and for the 8% EPR/PP blend in excess of 23 mm. The situation for the other two blends tested according to the *J*-procedure is even worse. The sample thickness for the 16% EPR/PP blend should be 400 mm and 675 mm for the 20% EPR/PP blend. The simple fact that the injection machine necessary to mold such thick samples does not yet exist means it would be absurd to compare hypothetical fracture results obtained on samples of such thickness. The structure of the blend (particle size and morphology) and the crystallization condition would be totally different from those of the material molded to the typical industrial thickness (few millimeters).

Other complications when applying fracture mechanics to polymers arise from strain softening and viscoelasticity.[24] Furthermore, for rubber toughened polymers in which the second phase particles undergo cavitation, the formation of microvoids almost completely obliterates the differences between the size of the plastic zone in plane stress and that corresponding to plane strain.[23] For similar reasons (void formation near the crack tip), and the same is true of pure polymers undergoing crazing, the material in the craze zone is in plane stress; consequently, these types of polymers are relatively insensitive to specimen thickness. Even non crazing polymers like poly(vinyl chloride) (PVC) and polycarbonate (PC) do not show thickness dependence.[24]

For the reasons stated above, in the current state of development of the fracture mechanics of polymers, the authors believe that the data presented in this work are representative, with a good degree of approximation, of the real fracture resistance of the blends in this study.

For rubber toughened polymers, the main part of the fracture energy is consumed by deformation processes, such as dilatational shear banding and multiple crazing, following particle cavitation or debonding. In order to facilitate the discussion of the SEN-3PB fracture specimens, the schematic representation given in Figure 10 can be helpful. The fracture surfaces of all specimens contain five distinct regions, the saw

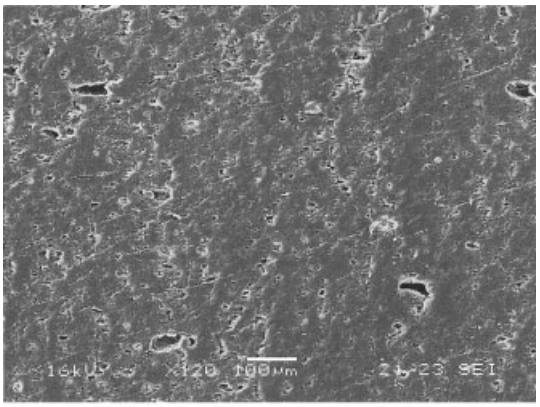

(a)

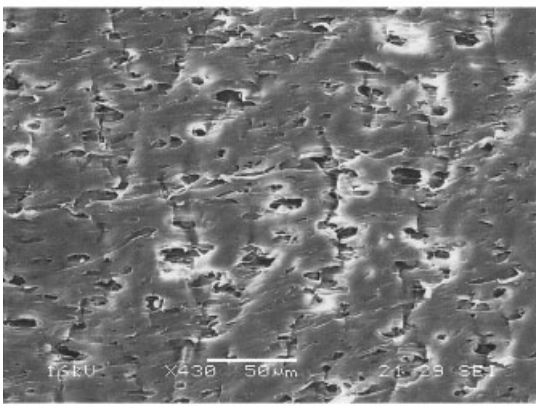

(b)

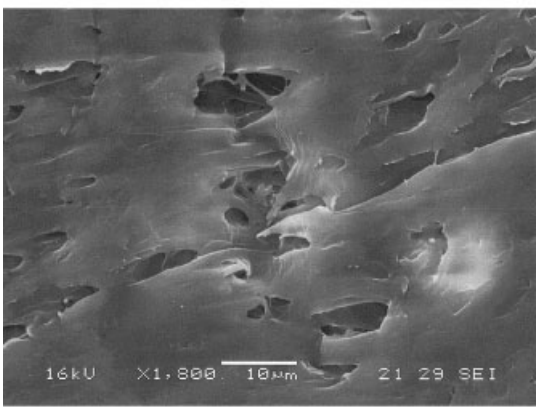

(c)

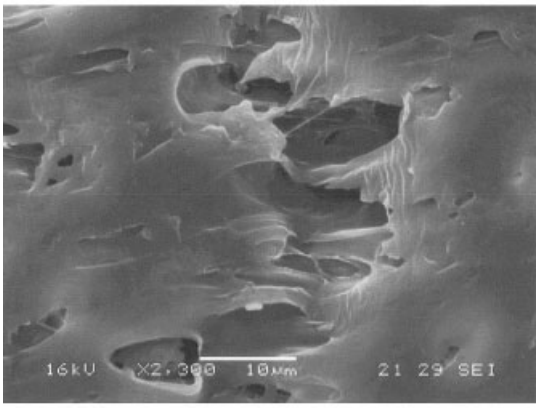

(d)

Figure 7 SEM micrographs of polished surfaces of tensile specimens of PP/EPR (20 wt %) blend, showing (a) a general view of the damage zone and (b–d) close-ups of (a).The loading direction is horizontal.

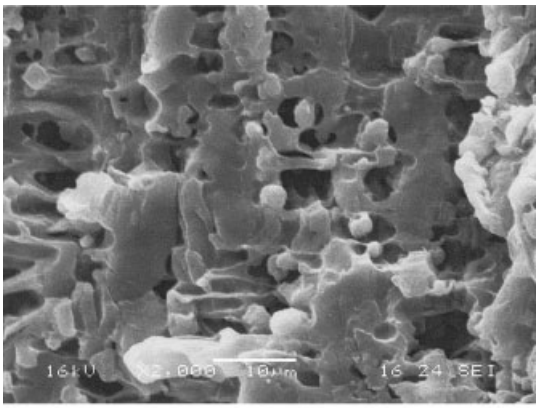

(a)

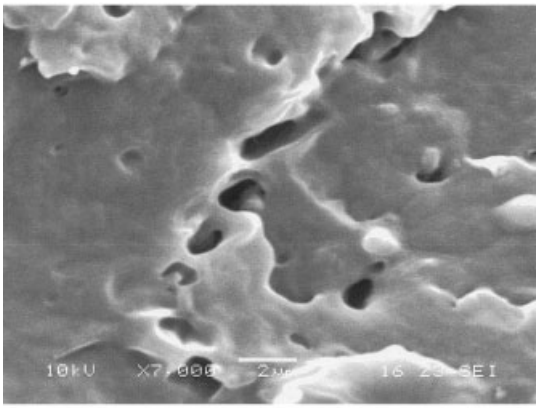

(b)

Figure 8 SEM micrographs of surfaces of tensile specimens of PP/EPR (20 wt %) blend fractured along the draw direction, showing (a) elongated voids and (b) dilatational band.

cut, the razor cut, the starter crack, the slow fracture stress whitened zone (SWZ), and the fast fracture zone. During a SEN-3PB test, the load rises to a maximum, then drops as the crack propagates through the sample. During the initial, rising part of the load-displacement curve, in pure PP and elastomer-toughened PP, a SWZ (also called damage zone) develops ahead of the pre-crack. For an unstable plane strain fracture, the rising load portion accounts for most of the total energy necessary to propagate the crack; thus the SWZ is directly related to the fracture mechanism responsible for energy absorption. Indeed, the stress whitening zone is due to the scattering of visible light and can be attributed to the various processes that can take place in the damage zone, such as matrix crazing, matrix shear yielding, rubber cavitation, and rubber/

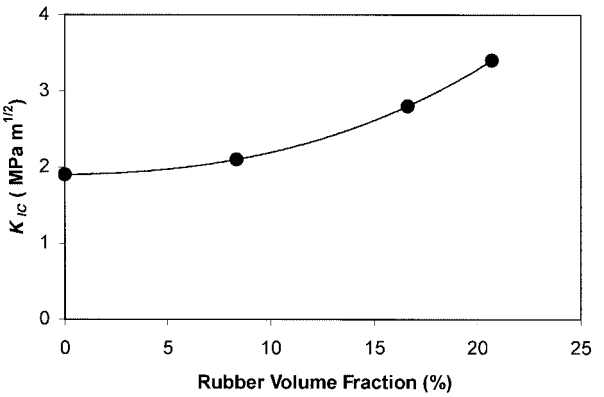

Figure 9 Dependence of fracture toughness (K_{IC}) on rubber content.

matrix debonding. The variation of SWZ width increases progressively with rubber content. The amount of dissipated energy is proportional to the SWZ extension in front of the crack tip, whose size depends on the yield strength and fracture toughness of the material.[24] Figure 11 shows that the variation of the width (h) of the crack tip SWZ of PP and its blends, studied in this work, follows the Irwin relation for the plastic zone size:[24]

$$h = 1/(2\pi)(K_{IC}/\sigma_y)^2 \quad (7)$$

Figure 11 also shows that eq. (7) fits our data fairly well.

This result implies that the SWZ strictly corresponds to the plastic zone in front of the starting crack. Upon increasing the rubber content, the fracture toughness increases, while the yield stress decreases. This leads to a spreading of the plastic zone and to an enhancement of the energy of dissipation, although the size of the SWZ can also be dependent on other parameters, such as temperature and test speed.

Microscope analysis of 3-PB specimens after fracture

SEM micrographs [Fig. 12(a,b)] show the fracture surface of PP/20 wt % EPR, in slow (SWZ) and fast

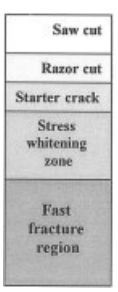

Figure 10 Schematic representation of fracture surface of three-point bending specimen.

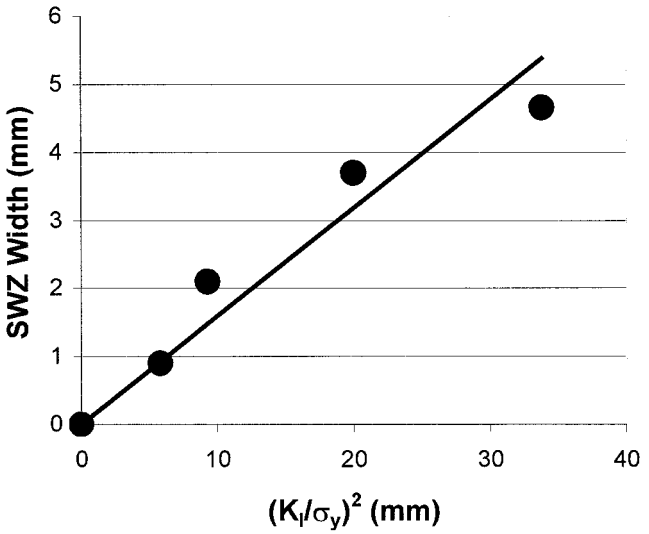

Figure 11 Variation of SWZ width with $(K_I/\sigma_y)^2$ for pure PP and its blends (yield stress values are taken from ref. 10). The line in the figure corresponds to the Irwin approximation.

regions, respectively. As can be seen, there are some voids that are not fully spherical but rather approach a polyhedral shape. By measuring their size from the pictures [Fig. 12(a,b)], it is found that the cavities in the slow crack growth region are larger than those in the fast crack growth region (about 1.5 times). This proves that, in the slow crack SWZ, rubber particle cavitation and growth have occurred, although in the same zone some matrix/rubber debonding is also observed [Fig. 12(c)]. In the last micrograph, cavity growth and coalescence are clearly visible.

Up to now, it has been shown that, for the rubber-toughened PP studied in this work, the stress whitening zone mainly includes particle cavitation with some matrix/rubber debonding. Figure 13 shows typical bending moment displacement curves for pure PP and its blends in 3-PB experiments, and Figure 14(a–d) shows optical micrographs of the side surface of the near crack tip area for a specimen of PP/20 wt % EPR blend. It should be noted that the onset of nonlinearity in the curve is associated with the formation of a large number of craze-like features in front of the notch tip. It was found that, at the beginning of deformation, these craze-like deformation zones start to appear at the notch tip for an applied bending moment of about 60% of the maximum reached before fracture (point A on Fig. 13). Craze-like features are clearly visible in Figure 14(a). Figure 14(b) illustrates the blend at point A on Figure 13 under dark field light. The development of the SWZ around the notch is shown in this picture. Increasing the applied load causes spreading of the SWZ out. Figure 14(c) shows the growth of craze-like bands under bright and dark field light respectively (point B on Fig. 13).

For further elucidation of the nature of the craze-like behavior in front of the notch, SEM analysis was

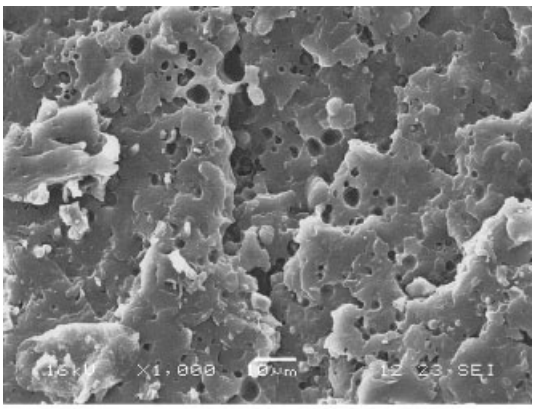

(a)

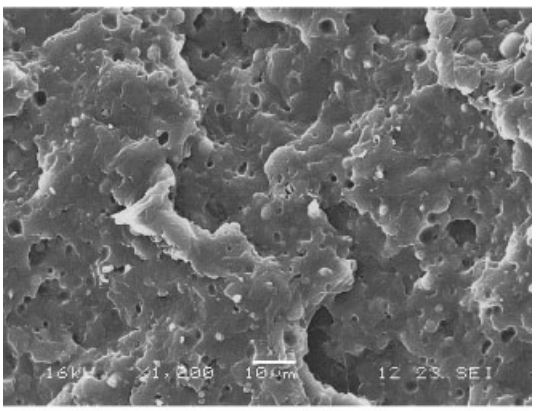

(b)

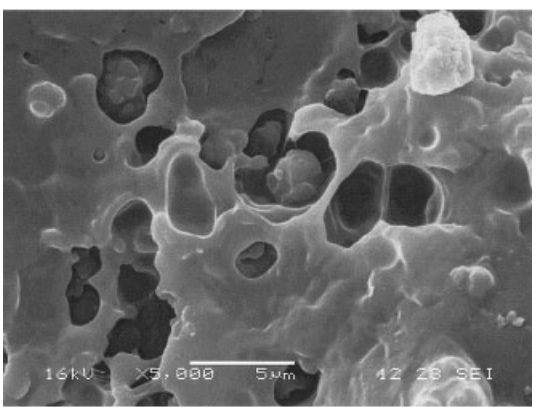

(c)

Figure 12 SEM micrographs of fracture surface of PP/20 wt % EPR blend with emphasis on (a) slow crack growth region, (b) fast crack growth region and (c) matrix/rubber debonding in slow crack growth region.

carried out. Figure 15(a–c) shows SEM micrographs taken from the polished surfaces of 3PB specimens (corresponding to point B on Fig. 13). As can be seen, craze-like features initiate from the notch tip and rubber particles and propagate in different directions [Fig. 15(a)]. Figure 15(b) is a close-up of Figure 15(a). It seems that there is a relationship between cavitation and craze-like damage. In fact, Figure 15(c) shows a combination of both craze-like bands and cavitation. In fact, craze-like band propagation appears to be associated with cavitation. Hence, one may conclude that the mechanism of this craze-like propagation is repeated cavitation.

Microscope analysis of 4-PB specimens after fracture

In order to better understand the mechanism of fracture, it is also important to consider the results of DEN-4PB tests. Figure 16(a,b) shows the SEM micrographs of the damage zone near a crack tip on 4PB samples of pure PP. As can be seen, the damage zone in pure PP is composed of only a few crazes.

Figure 17(a–d) shows SEM micrographs of the side surfaces of the damage zones in front of the pre-cracks in PP blends under 4PB test. Figure 17(b–d) are close-ups of Figure 17(a). As can be seen, craze-like features are present at the crack tip. They seem to be associated with particle cavitation and debonding. With regards to our results in tensile tests and the observation of birefringence in cross-polarized light optical microscopy, it appears that this type of craze-like structure that grows by repeated cavitation is a form of dilatational (shear) bands (Fig. 18). In the following section, we will try to elucidate this subject.

Discussion

Pure polypropylene is a thermoplastic polymer that is known to undergo both shear yielding and crazing behavior, depending on temperature and testing conditions. At a given temperature, there is a critical strain rate above which crazing is the dominant mode of deformation. In addition, at a given strain rate,

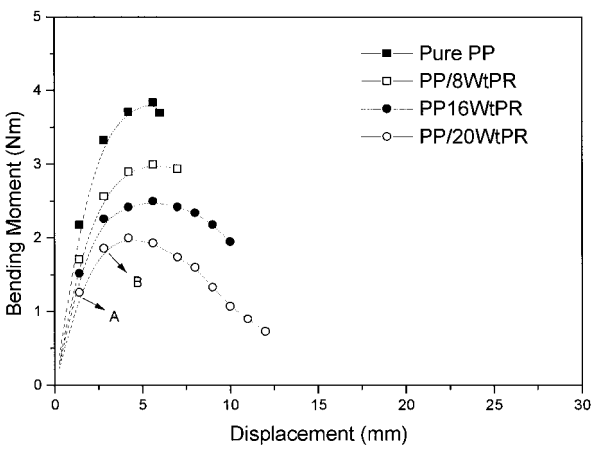

Figure 13 Effect of rubber content on bending moment-displacement curves of PP blends.

there exists a critical test temperature that divides crazing from shear yielding behavior.

In contrast to the tendency of pure PP toward crazing and shear yielding, we have shown that, for the PP blends studied in this work, the dominant mechanism of deformation in tension and fracture tests is massive dilatational shear banding due to repeated cavitation, while, particularly in fracture tests, some particle/matrix debonding is also observed. This means that the debonding stress is lower than the cavitation stress, which in this system may be estimated to be a critical hydrostatic stress of about 2.5 MPa (corresponding to a tensile stress of 7.5 MPa) by considering the relatively large particle size (>4 μm) and the typical properties of the EPR copolymer.[23] Since the yield stress of the PP blends is within the range 18–22 MPa, debonding and cavitation occur well within the elastic regime for all of these materials. This is consistent with the observation of craze-like features near the crack tip, which appear to result from high shear localization in the ligament between debonded/cavitated particles in dilatational bands. The rather large particle size and the limited rubber/matrix adhesion result in a relatively limited number of dilatational shear bands, formed well below the yield stress, which tend to localize since the rest of the material is still in the elastic region. Moreover, shear localization prevents the formation of a diffuse ('percolated') network of dilatational shear bands and leads to premature unstable crack propagation. In fact, since debonding and cavitation occur too early, in the presence of high strain rates or low temperatures, these bands may behave as precursor cracks. When one of these cracks becomes unstable, a brittle fracture occurs with limited energy absorption. As a consequence, this material fails to provide the expected high level of toughness.

For the PP blends studied in this article, the observed craze-like structures appear to be highly localized dilatational shear bands. Comparing the results obtained in tension and fracture tests, it appears that dilatational bands are more localized when the dilatant component of the stress tensor is larger, as near the crack tip. This obviously favors cavity growth and an increase in thickness of the dilatational band over an increase in band length or nucleation of new bands. This increases the severity of localization of these damage bands.

The localization of deformation is probably also related to the rather large interparticle distance found

Figure 14 Optical microscopy of polished surfaces of impact specimens after some deformation under three-point bending test:(a) nucleation of craze in notch tip under bright field (point A on Fig. 13), (b) same as (a) but under dark field, (c) craze growth in length and nucleation of new crazes under bright field (point B on curve).

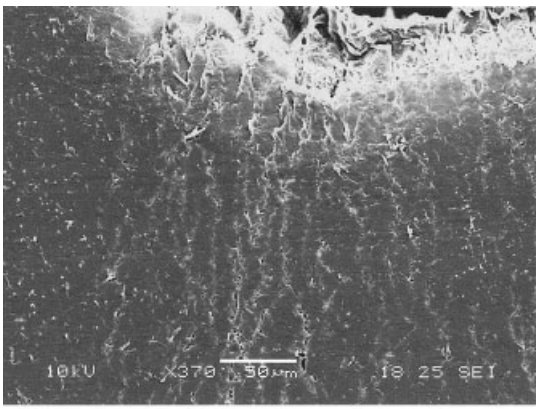

(a)

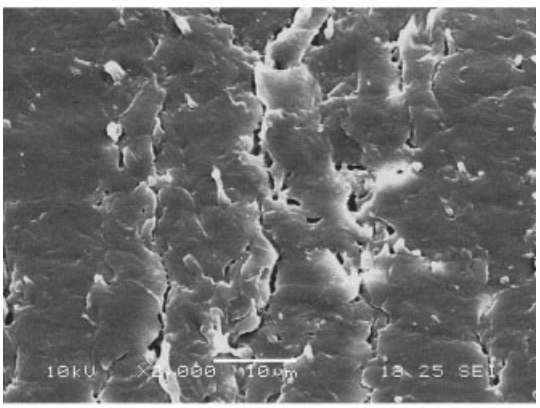

(b)

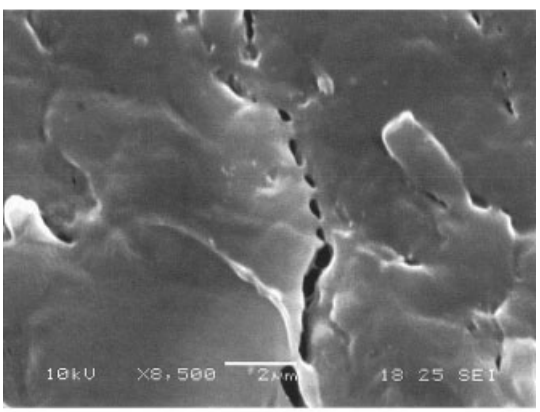

(c)

Figure 15 SEM micrographs of polished surface of three-point specimen (point B on Fig. 13): (a) initiation of crazes in front of notch tip, (b) close-up of (a), (c) craze due to repeated cavitation.

in this system. Lazzeri has recently proposed that rubber stretching plays a substantial role in the stabilization of dilatational bands during their propagation.[1] Recent experimental papers support this theoretical prediction.[25,26] In particular, a NMR imaging study of stress-induced material response carried out by Adriaensens and coworkers[25] on rubber modified nylon has shown that the toughness of the material is strongly related to the load bearing capacity of the cavitated rubber particles in dilatational bands. In fact, after cavitation, the biaxial stretching of the rubbery layer attached to the cavity walls[26] can stabilize the growing dilatational band by absorbing elastic energy, delaying strain localization and premature failure. Under impact conditions, thermal failure may also occur in the ligaments between particles. Figure 18 shows a diagram of the propagation step of a dilatational band by repeated cavitation of the rubber particles, followed by plastic deformation of the intervening glassy ligaments. When propagation is very fast, the temperature rise in the ligament, due to stretching, can bring the temperature close to or above the T_g value of the glassy phase of the polymer. The work required for further deformation becomes very small, and only rubber stretching can give a substantial contribution to energy dissipation.

Lazzeri[1] has also shown that the stabilizing effect of elastomeric particles will be stronger when the interparticle distance decreases, since small particles un-

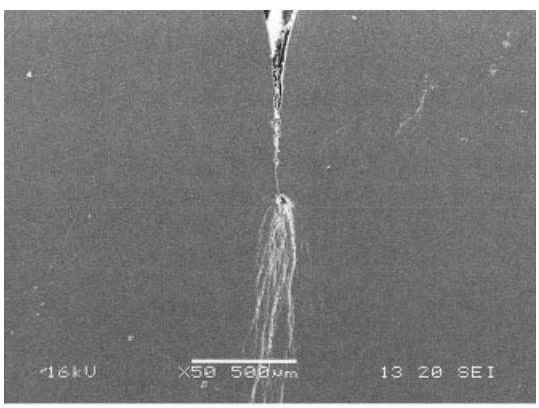

(a)

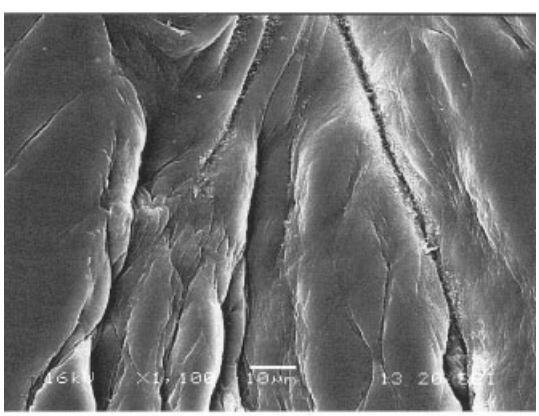

(b)

Figure 16 SEM micrographs of polished surface of four-point bending specimen of pure PP: (a) damage zone in front of pre-crack, (b) interaction between crazes and microstructure.

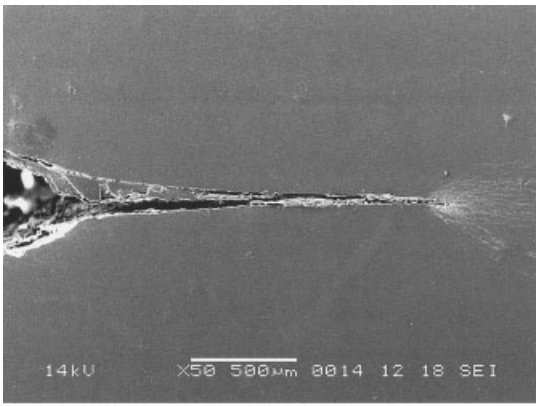

(a)

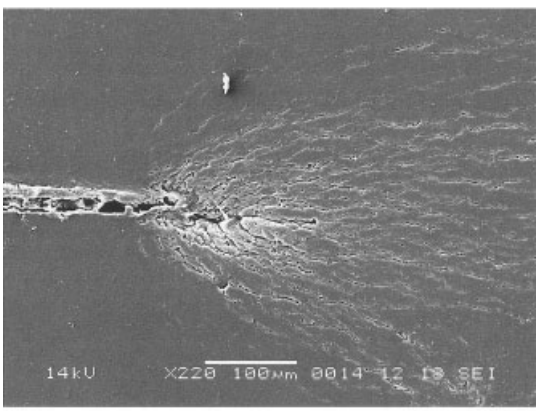

(b)

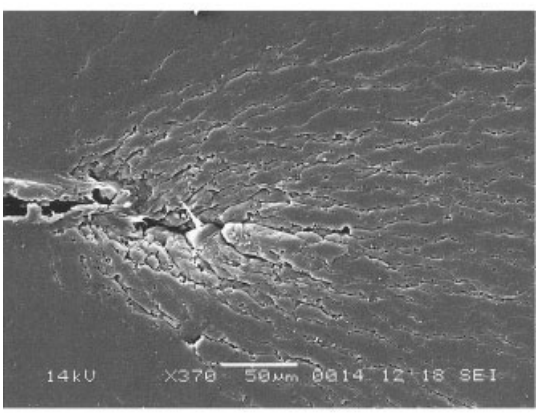

(c)

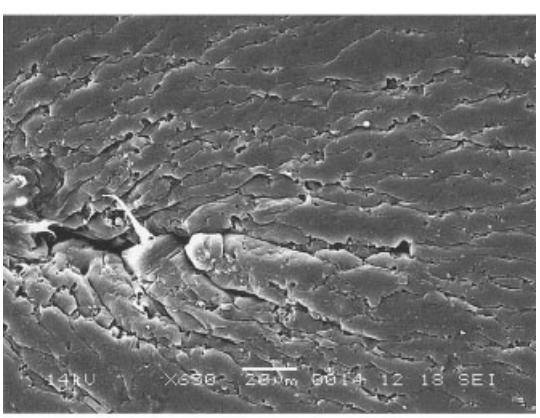

(d)

Figure 17 SEM micrographs of polished surface of four-point bending specimen of PP/20wt % rubber blend: (a) damage zone in front of pre-crack, (b–d) close-ups of (a).

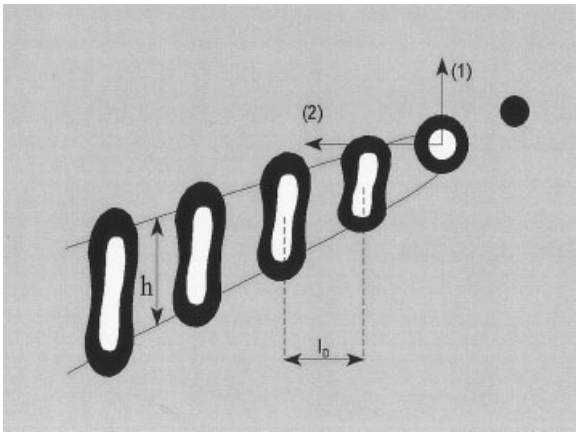

Figure 18 Diagram of propagation mechanism of dilatational band by repeated cavitation of the rubber particles, followed by plastic deformation of the intervening ligaments.

dergo higher straining than larger particles as the dilatational band thickness increases. Moreover, a larger elastic shear modulus of the rubber, by means of a slight crosslink, due to either physical or chemical constraints, enhances the shear properties of the rubber and therefore is also important in band stabilization.[1] This prediction is confirmed by the experimental findings of Adriaensens and coworkers[25] in rubber modified nylon. They found that the blend in which the rubbery phase had superior elastic properties, due to physical and topological constraints, also showed enhanced toughness and a more extended plastic zone ahead of the crack tip. Also, Riccò and coworkers[26] reported that, in rubber toughened PP, ethylene-butene rubber (EBR) was more effective than EPR in enhancing the fracture toughness of PP blends, despite a lower tendency to cavitate. Improvement of the fracture resistance was also achieved by the same authors by increasing the molecular mass of the elastomers. These observations agree very well with the model proposed by Lazzeri[1] on the stabilizing role exerted by stretched rubber particles after cavitation. In fact, by delaying damage localization, these particles enable dilatational bands to develop further into the material away from the notch, leading to a more pronounced delocalization of energy and to a larger shielding effect by a more extended plastic zone. From this point of view, rubber/matrix debonding might even be more damaging than premature particle cavitation, since a debonded particle cannot exert any stabilizing role at all.

In the ideal case, small cavitated rubber particles between the matrix ligaments, by stretching elastically, can substantially delay damage localization, enabling more dilatational bands to form and develop

further into the material away from the notch, leading to a pronounced delocalization of energy and to a larger shielding effect by a larger plastic zone.

For the PP/EPR blends, a smaller particle size and a stronger rubber/matrix adhesion than that used in this work is thought to be extremely important if a high fracture resistance is to be achieved. The two conditions will lead to cavitation at higher stress levels near the yield point of the matrix. This will favor the formation of a diffuse network of a large number of dilatational shear bands corresponding to a high density of energy dissipated in the damage (whitened) zone.

CONCLUSIONS

In order to study the role of rubber particles on the mechanical properties and the mechanism of deformation of PP, DSC, tensile tests, 3PB and 4PB tests, and microscopy evaluations were carried out.

The results of DSC analysis illustrate that the addition of EPR to PP has no significant effect on the heat of melting and the degree of crystallinity of the PP phase in the blend. The results of tensile tests show that yield strength and modulus of elasticity decrease with increasing weight percent of EPR. Further deformation or increase of rubber content causes an increase of damage intensity and promotes damage intersection. The results of the 3PB test show that fracture toughness increases with rubber content.

Microscope studies show that the dominant mechanism of deformation in tensile specimens of PP/EPR blends is massive shear dilatational banding caused by repeated cavitation. SEM analysis also shows evidence of rubber particle cavitation and microvoiding due to debonding in the slow crack propagation zone near the crack tip in the PP blends studied in this work, associated with craze-like structures in the presence of extensive shear yielding. These craze-like structures are suggested to be a more highly shear localized version of the dilatational bands observed under tension. Furthermore, SEM analysis shows that the mechanism of propagation of these craze-like structures in PP blends is repeated debonding and cavitation of the rubber particles. Shear localization of the dilatational bands is suggested to be related to the large particle size that causes debonding and cavitation to occur at low applied stresses when the material is well below the yield stress. The resulting dilatational bands form prematurely, and shear deformation localizes in the ligaments between neighboring cavities. This localization prevents the formation of a diffuse network of dilatational bands, severely limiting the possibility of achieving high values of the plastic energy density dissipated in the damage zone. The overall fracture toughness of the material is thus seriously affected.

References

1. Lazzeri, A. Proceedings of the 10th International Conference on Deformation, Yield and Fracture of Polymers, Cambridge, UK, April 7–10, 1997, p 75.
2. Woishnis, W. Polypropylene; PDI Publisher: New York, 1998.
3. Karger-Kocsis, J. Polypropylene: Structure, Blends and Composites; Chapman and Hall: London, 1995.
4. Gaymans, R. J. In Polymer Blends; Paul, D. R., Bucknall, C. B., Eds.; John Wiley & Sons: New York, 2000; Chapter 25.
5. Liang, J. Z.; Li, R. K. Y. J Appl Polym Sci 2000, 77, 409.
6. Yokoyama, Y.; Riccò, T. J Appl Polym Sci 1997, 66, 1007.
7. Wu, S. J Polym Sci, Polym Phys Ed 1983, 21, 699.
8. Zebarjad, S. M.; Bagheri, R.; Lazzeri, A. Plastics, Rubber and Composites 2001, 30, 370.
9. Zebarjad, S. M.; Lazzeri, A.; Bagheri, R.; Seyed Reihani, S. M.; Forunchi, M. J Mater Sci Letters 2002, 21, 1007.
10. Zebarjad, S. M.; Lazzeri, A.; Bagheri, R.; Seyed Reihani, S. M.; Frounchi, M. Material Letters 2003, 24, 105.
11. ESIS (European Structural Integrity Society), A Linear Elastic Fracture Mechanics Standard for Determining K_c and G_c for Plastics, 1990.
12. ESIS (European Structural Integrity Society), Recommendation for Determining the Fracture Resistance of Ductile Materials, 1991.
13. Holi, A. S.; Kambour, R. P.; Hobbs, S. Y.; Fink, D. G. Microstruct Sci 1979, 7, 357.
14. Isasi, R. J.; Mandelkern, L.; Galante, M. J.; Alamo, R. G. J Polym Sci, Polym Phys Ed 1999, 37, 323.
15. Chou, C. J.; Vijayan, K.; Kirby, D.; Hiltner, A.; Baer, E. J Mater Sci 1998, 23, 2521.
16. Friedrich, K. Advances in Polymer Science 1983, 52/53, 226.
17. Nielsen, L. Mechanical Properties of Polymers; Marcel Dekker: New York, 1972.
18. Lazzeri, A.; Bucknall, C. B. Polymer 1995, 36, 2895.
19. Chiang, W.-Y.; Yang, W.-D.; Pukanszky, B. Polym Eng Sci 1992, 32, 641.
20. Jackson, G. V.; Orton, M. L. In Particulate-Filled Polymer Composites; Rothon, R., Ed.; Longman: London, 1995; Chapter 9.
21. Chow, T. S. J Polym Sci, Polym Phys Ed 1978, 16, 959.
22. Gloagen, J. M.; Heim, P.; Gallard, P.; Lefebvre, J. M. Polymer 1992, 33, 4741.
23. Lazzeri, A.; Bucknall, C. B. In Toughened Plastics: Advances in Modeling and Experiments; Pearson, R., Sue, H.-J., Yee, A. F., Eds.; Oxford University Press: New York, 2000; Chapter 2.
24. Anderson, T. L. Fracture Mechanics: Fundamentals and Applications, 2nd ed.; CRC Press: Boca Raton, FL, 1995.
25. Adriaensens, P.; Storme, L.; Carleer, R.; D'Haen, J.; Gelan, J.; Litvinov, V. M.; Marissen, R.; Crevecoeur, J. Macromolecules 2002, 35, 135.
26. Yokoyama, Y.; Riccò, T. Polymer 1998, 39, 3675.